



Electrospinning fabrication of porous BaMnO₃ nanofibers: analysis of structure, surface morphology and optical property

Mohammad Zare¹ · Hossein Mahmoudi Chenari¹

Received: 3 June 2018 / Accepted: 22 August 2018 / Published online: 1 September 2018
© Springer-Verlag GmbH Germany, part of Springer Nature 2018

Abstract

The electrospinning technique has been successfully employed for the fabrication of porous BaMnO₃ nanofibers, followed by different thermal treatment. The samples were studied by X-ray diffraction (XRD), scanning electron microscopy/energy-dispersive spectroscopy (SEM/EDX), Fourier transform infrared (FT-IR) spectroscopy, and diffuse reflectance spectroscopy (DRS). The XRD pattern shows that the organics were completely removed in sample calcined at 800 °C and the hexagonal BaMnO₃ nanofibers were obtained. The microstructural parameters such as crystallite size and lattice strain contributions to line broadening were estimated using Williamson–Hall (W–H) analysis. The morphology and average diameters of the prepared nanofibers were estimated from the SEM images. The SEM images of the calcined samples show porous structure. The optical properties were studied using UV–Vis diffuse reflectance spectroscopy (DRS) and photoluminescence (PL) spectra. The optical bandgap of the calcined nanofibers decreased with an increase in calcination temperature from 700 to 800 °C. The PL spectrum shows that BaMnO₃ nanofibers increased the radiative centers. We thus conclude that BaMnO₃ nanofiber shows luminescent property.

1 Introduction

In recent years, considerable amount of work has been devoted to the fabrication of one-dimensional (1D) nanofibers [1–7]. Among various techniques for the fabrication of nanofibers, the electrospinning technique allows the production of nanofibers with diameters down to 100 nm which can be controlled by tuning spinnable solution. In this method, the fibrous web can be produced via uniaxial stretching of a polymeric solution. In the last decade, multiferroic nanostructures have received a great deal of interest for their potential applications in multiple-state memory devices, ferromagnetic resonance devices, piezoelectric devices, and broadband magnetic field sensors [8–10]. Among all multiferroic nanostructures, considerable attention has been focused on the development of multiferroic nanofibers. Xie et al. [11] fabricated multiferroic single-phase nanofibers such as PZT-CFO, PZTNFO, and BiFeO₃ (BFO) composite nanofibers along with theoretical analysis and structural

study. Baji et al. [12] reported the ferroelectricity and ferroelectric domain structures of multiferroic bismuth ferrite fibers. Strontium hexaferrite (SrFe₁₂O₁₉) nanofibers with high saturation magnetization were investigated by Gu et al. [13]. Vijayakumar et al. [14] reported the dielectric studies, linear and non-linear optical properties of ZnO/BaO composite nanofibers. The motivation of present work is fabrication and characterization study of the barium manganate, BaMnO₃, nanofibers. BaMnO₃ is a class of well-known perovskite-based material that displays n-type semiconductor behavior [15–17].

To the best of author's knowledge, there is no report to focus on the microstructure analysis and optical properties of BaMnO₃ nanofiber, prepared at different calcination temperatures. So, this research aims microstructure analysis and optical evaluation of BaMnO₃ nanofibers. The produced BaMnO₃ nanofibers were further characterized using XRD, SEM, EDX, FT-IR, DRS, and PL.

2 Experimental procedure

Poly(vinylpyrrolidone) (PVP, $M_w = 1,300,000$), barium acetate [Ba(CH₃COO)₂], and manganese acetate [C₄H₆MnO₄·4H₂O] were purchased from Merck and

✉ Hossein Mahmoudi Chenari
mahmoudi_hossein@guilan.ac.ir;
h.mahmoudiph@gmail.com

¹ Department of Physics, Faculty of Science, University of Guilan, Namjoo Ave, Po Box 41335-1914, Rasht, Iran

Sigma-Aldrich Co. without further purification. Ethanol and acetic acid were used as solvent. To prepare BaMnO₃ nanofibers, 0.0025 mol of Ba(CH₃COO)₂ and 0.0025 mol of Mn(CH₃COO)₂·4H₂O were added into 3 mL of acetic acid under vigorous stirring. Subsequently, 1 g of PVP was dissolved in 6.75 mL ethanol and stirred for 45 min. The two solutions were then mixed together under vigorous stirring for 15 h to form a viscous solution. The prepared solutions were loaded into plastic syringes with a constant feed rate of 0.5 ml/h by applying 12 kV at an electrode distance of 12 cm. The as-prepared nanofibers were dried in the oven for 1 h at 70 °C. Finally, the fibers were calcined at different temperatures (500 °C, 700 °C and 800 °C) for 2 h to eliminate the organics. The samples calcined at 500 °C, 700 °C and 800 °C are denoted by a, b, and c, respectively. Calcination was carried out using Exciton furnace (Exciton Co. Ltd., Iran, <http://www.exciton.ir>) and the electrospinning process was performed using Electroris (eSpinner NF CO-N/VI, Iran, <http://www.anstco.com>) with a high voltage, 1–35 kV, and a syringe pump within a controllable range, from 0.1 to 100 mL/h. The obtained nanofibers are characterized by various techniques.

The phase composition of the BaMnO₃ nanofibers was characterized by X-ray diffraction using a Cu-K α radiation ($\lambda = 1.5406 \text{ \AA}$), recorded by INEL EQUINOX 3000 X-ray Diffraction System, operated at 40 kV and 35 mA. The surface morphology of the prepared nanofibers was studied by scanning electron microscope using Seron Technology-AIS 2100. The elemental analysis of the BaMnO₃ nanofibers was recorded by means of energy-dispersive X-ray (EDX) (Tescan Vega-II XMU SEM). The infrared spectra were collected using an ALPHA II, Bruker FT-IR spectrometer in the range

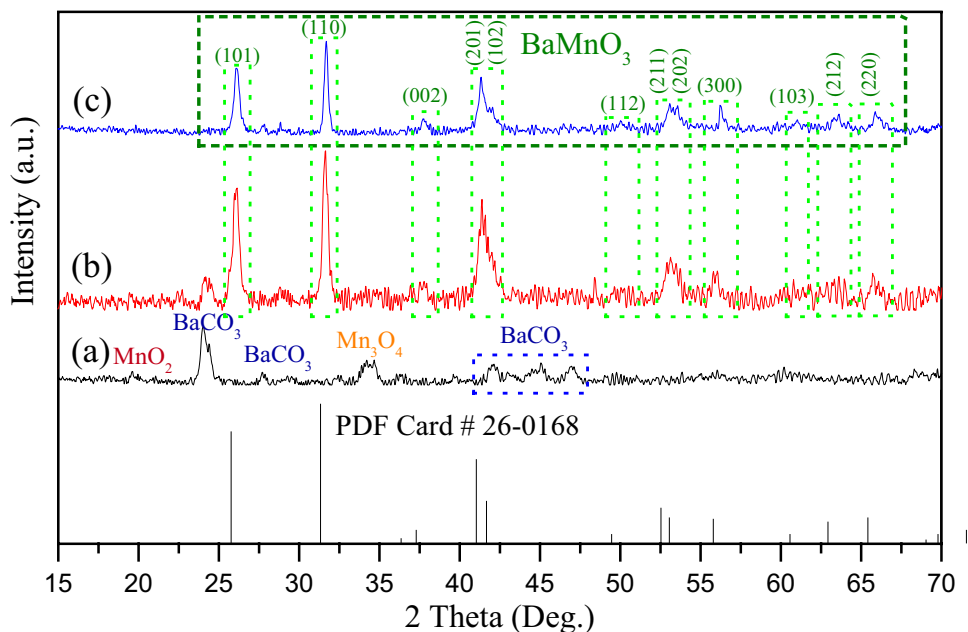
400–4000 cm⁻¹. Diffuse reflectance spectra were measured by Scinco S-4100 UV–visible spectrophotometer. In the end, photoluminescence measurements were performed by means of Cary Eclipse Fluorescence spectrophotometer with excitation wavelength of 250 nm at room temperature.

3 Results and discussion

3.1 Structure and morphological analysis

Figure 1a–c shows the XRD diffraction pattern of the BaMnO₃ nanofibers calcined at different temperatures 500 °C, 700 °C and 800 °C, respectively. It is evident from the XRD pattern that barium manganese phase is not formed at 500 °C and a mixture of the BaCO₃ and MnO₂ phases was observed. By increasing the calcination temperature, the peak intensity of BaCO₃ and MnO₂ phases decreased and a single phase of BaMnO₃ nanofibers appeared at 800 °C with high intensity. Well-defined diffraction peaks corresponding to (101), (110), (002), (201), (102), (112), (211), (202), (300), (103), (212), and (220) planes match well with the hexagonal phase of BaMnO₃ according to the JCPDS card no. 26–0168 with space group: P 63/m mc. The diffraction peaks become intense with an increase in the calcination temperature, induced by the crystallite growth. The patterns that resulted from Rietveld refinement with Maud and Fullprof software for BaMnO₃ nanofibers calcined at 700 °C and 800 °C are shown in Fig. 2. The Rietveld analysis has been applied to determine the lattice parameters “a” and “c” (see Table 1).

Fig. 1 Room-temperature XRD patterns of the BaMnO₃ nanofibers calcined at **a** 500 °C, **b** 700 °C and **c** 800 °C



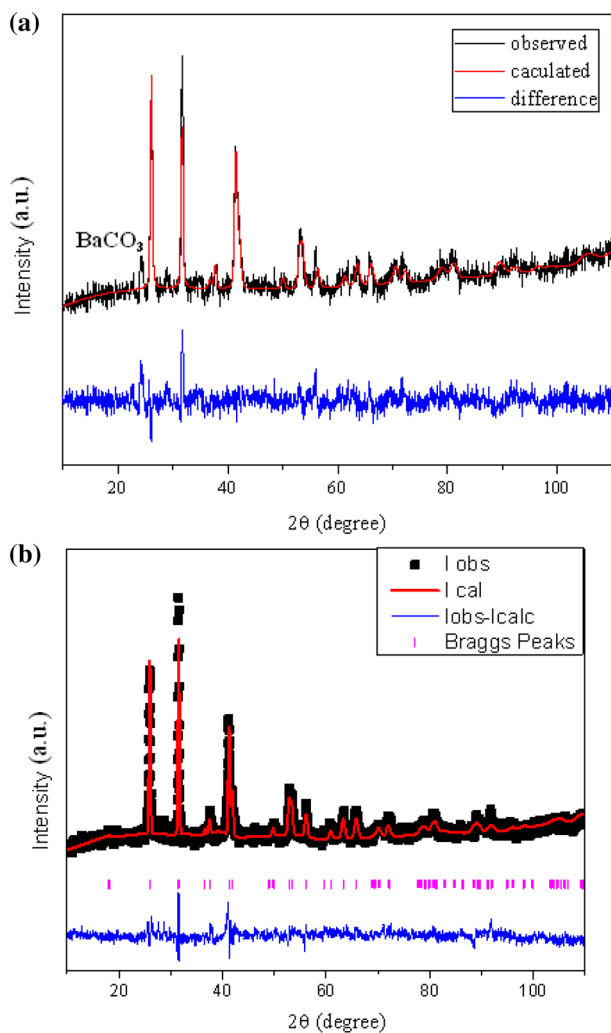


Fig. 2 Rietveld refinement patterns of X-ray diffraction for BaMnO₃ nanofibers calcined at 700 and 800 °C. The black, red and blue patterns show the observed, calculated and the differences between the intensities observed and the intensities calculated of X-ray diffraction pattern

Microstructure parameters such as average crystallite size and lattice strain were estimated using Williamson–Hall analysis (W–H) [18] given by

$$\beta_{hkl} \cos \theta = (k\lambda/D) + 4\epsilon \sin \theta \quad (1)$$

where β_{hkl} shows the total X-ray peak broadening due to crystallite size and lattice strain contributions. The instrumental-corrected broadening, β_{hkl} , was calculated as

$$B_{hkl}^2 = [(\beta_{hkl}^2)_{\text{Measured}} - (\beta_{hkl}^2)_{\text{Instrumental}}] \quad (2)$$

The dislocation density (dislocation line length per unit volume), δ , was estimated using

$$\delta = \frac{1}{D^2} \quad (3)$$

The average crystallite size and lattice strain are shown by D and ϵ , respectively. The dislocation density was found to decrease with increase in calcination temperature as the crystalline quality of BaMnO₃ nanofibers was increased. In the W–H approach, the lattice strain is assumed to be isotropic in all crystallographic directions. Figure 3b–c shows the measured values of $\beta_{hkl} \cos \theta$ as a function of $4\sin \theta$ for BaMnO₃ nanofibers calcined at 700 °C and 800 °C, respectively. The slope and y-intercepts of the fitted line represent the strain and crystallite size value, respectively. The scattered data around the linear fit show the presence of the defects such as dislocations or the highly distorted environment in nanofiber structure. With increase in the calcination temperature, the lattice strain decreased due to the reduced surface defects and the enhanced crystallinity of nanofibers. Microstructure parameters are given in Table 1. The calculated average crystallite size of the BaMnO₃ nanofibers increased with calcination temperature due to an increase in the nucleation rate of the particles and the crystallite growth.

Figure 4a–c shows the surface morphology and the diameter distribution of the as-prepared and calcined BaMnO₃ nanofibers using SEM analysis. The SEM images indicate the formation of smooth and regular electrospun samples and porous structure of the calcined nanofibers. The particle size distribution analysis shows fiber diameters ranging from 350 to 850 nm for as-prepared and calcined nanofibers, respectively. The number of porous BaMnO₃ nanofibers with diameter between 1000 and 1100 nm increased by increasing the calcination temperature to 800 °C due to increase in the nucleation rate of the particles. But the variations of nanofibers diameters were not significant as shown in a separate graph in Fig. 4. The surface morphology and the diameters of nanofibers can be controlled by thermal degradation of

Table 1 Microstructural parameters of the calcined BaMnO₃ nanofibers

Sample (calcination temperature, °C)	Lattice parameters (nm)		Average crystalline size, D (nm)		Average internal strain, ϵ ($\beta/4 \times \tan \theta$) $\times 10^{-3}$	Dislocation density, δ ($1/D^2$) $\times 10^{15}$ lin/m ²
	a	c	Scherrer	(W–H) model		
700	5.655117	4.770646	21.65	13.26	−1.52	5.68
800	5.673939	4.797863	25.51	20.67	−0.11	2.34

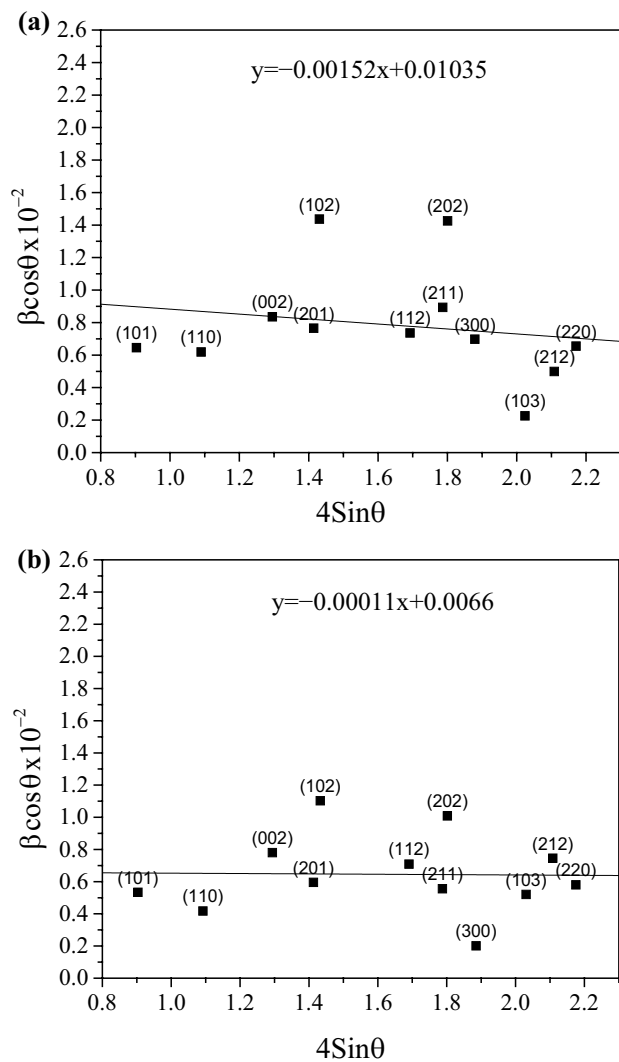


Fig. 3 The W–H plot of BaMnO₃ nanofibers calcined at **a** 700 °C and **b** 800 °C. The equation of the straight line is shown in the panel of image

PVP. The grain growth in BaMnO₃ nanofiber after decomposition of PVP is a thermal activation process, from which atoms diffuse to stable positions. So, the grain growth and coalesce increase the fiber diameter owing to increased diffusion rate due to the elevated calcination temperature. Thus, the diameter of the produced nanofibers became larger and a grainy structure was formed on the surface of fibrous web. So, one can conclude that increase in the fiber diameter of BaMnO₃ nanofibers can be attributed to the thermal activation process. A similar observation has been reported by other persons [19, 20]. Figure 5 shows the elemental composition of BaMnO₃ nanofibers calcined at 800 °C using the EDS method. The EDX spectrum indicates that Mn, Ba, and O are the main elemental species in BaMnO₃ nanofibers.

The room-temperature FT-IR spectra of the as-prepared and calcined BaMnO₃ nanofibers are shown in Fig. 6. The

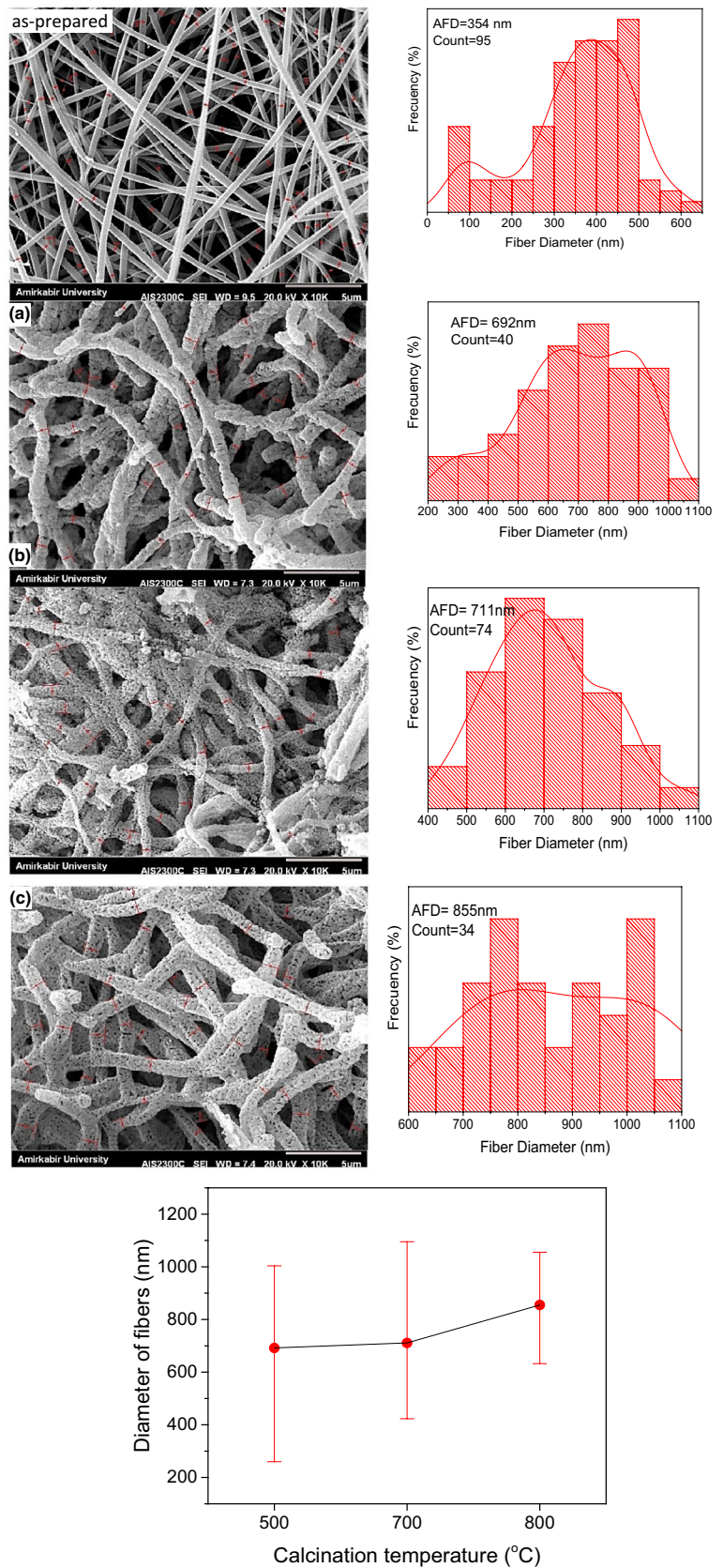
vibration mode at 3416–3437 cm⁻¹ can be assigned to the stretching vibration of hydroxyl group ($\nu_{\text{O-H}}$) (OH or H₂O) [21]. The absorption bands around 2923–2955 cm⁻¹ are due to carbon–hydrogen ($\nu_{\text{C-H}}$) bond stretching [15]. Band stretching of the C=O groups in the FT-IR spectra of the as-prepared sample appears in the spectral region 1662 cm⁻¹ [21]. The frequency band near 1421 cm⁻¹ corresponds to the presence of C–H stretch [15]. The observed absorption bands in the range 1385–1444 cm⁻¹ and 826–859 cm⁻¹ for calcined nanofibers can be assigned to the asymmetric stretching of (BaCO₃)(CO₃)⁻² [21], which decreases with increase in the calcination temperature. The peak located at 1024 cm⁻¹ is due to the C–O vibration mode. The absorption bands observed in the range 520–650 cm⁻¹ correspond to the stretching vibration of M–O bonds in BaMnO₃ [22]. The peak located at 489 cm⁻¹ can be attributed to the Mn–O–Mn bending vibration mode [22]. The absorption bands in the range 489–759 cm⁻¹ can be assigned to the vibration mode of Mn with O (M–O) [15, 21]. It is obvious from Fig. 6 that the absorption band intensity of PVP has been decreased at 800 °C.

3.2 Optical study

UV–Vis diffuse reflectance spectrum of the BaMnO₃ nanofibers calcined at 700 and 800 °C is shown in Fig. 7. The optical bandgap can be estimated from the maximum of the first derivative and intercept of the second derivative of the absorbance data versus energy axis. As can be seen in Fig. 7, the optical bandgap of the BaMnO₃ nanofibers decreased from 2.99 to 2.98 eV as the calcination temperature increased, due to increase in the nucleation rate of the particles within the nanofibers.

Figure 8 shows the photoluminescence (PL) spectrum of BaMnO₃ nanofiber under 250-nm excitation. Although BaMnO₃ does not show room-temperature PL emission and is not a luminescent material [15, 23], interestingly, BaMnO₃ nanofiber revealed photoluminescence emission peaks in the ultraviolet and visible ranges. BaMnO₃ nanofiber shows intense emission in the visible region. The strong line at 295 nm can be related to the localized states in the bandgap. PL spectrum also shows the broad emission bands with weak intensity emission due to the defects such as oxygen vacancies available in the lattice structure of BaMnO₃ nanofiber. Oxygen vacancies introduce a series of states within bandgap, which provide excitation. Luminescence emission is usually associated with the presence of structural disorder and formation of electronic levels in the bandgap that act as recombination center for the electron–gap pair. According to the previous reports [24–26], the visible blue emission peak observed in the PL spectrum of BaMnO₃ nanofibers could be due to 3P₂₀ to 3D₃ band transition of barium atom and the green emission

Fig. 4 SEM images of the as-spun and calcined BaMnO₃ nanofibers



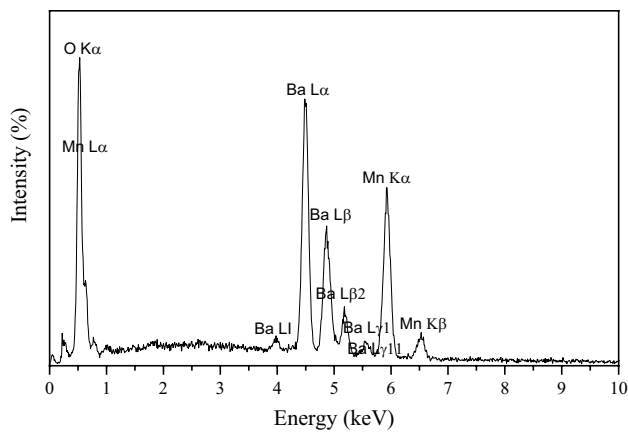


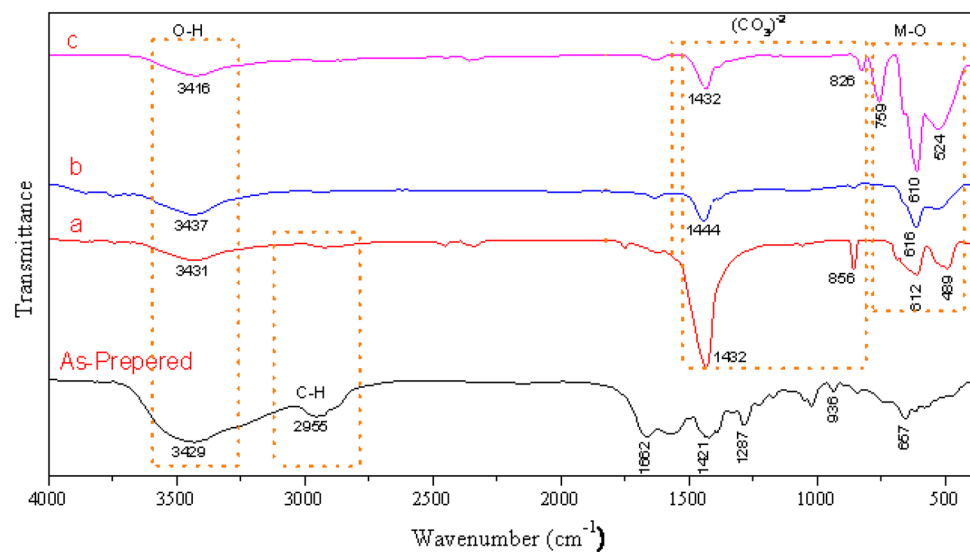
Fig. 5 Energy-dispersive X-ray spectrometer (EDX) spectrum for BaMnO₃ nanofibers calcined at 800 °C

bands can be ascribed to the $3P_0^0$ to $3D_1$ band transition. The reason why the fabricated BaMnO₃ nanofiber showed pronounced enhancement of the photoluminescence intensity can be related to a series of factors such as synthesis process (electrospinning), grain size distribution within the fibrous web and also small crystal size (in our case about 13 nm). Presence of structural defects including distortions, tensions and oxygen vacancies which are formed in the nanofiber structure during the preparation or after thermal treatments could be the other reason why BaMnO₃ nanofiber showed radiative centers and promoted excitation. So, we came to a conclusion from the PL spectrum that BaMnO₃ nanofiber shows luminescent property with emission peaks in the visible region which can be a useful candidate in optical application.

4 Conclusion

In summary, porous BaMnO₃ nanofibers were successfully synthesized by a simple electrospinning technique, followed by different thermal treatment. The effect of calcination temperature on the crystal structure, morphology and also optical properties of the produced nanofibers has been studied by X-ray diffraction analysis, scanning electron microscopy, Fourier transform infrared spectroscopy, UV–Vis diffuse reflectance spectroscopy, and the PL spectrum. X-ray diffraction pattern shows single hexagonal phase of BaMnO₃ with good crystallinity at 800 °C. SEM results indicate the formation of smooth and regular electrospun nanofibers and porous structure for samples after thermal treatment. The optical study shows that bandgap of the BaMnO₃ nanofibers decreases with increase in the calcination temperature. Interestingly, BaMnO₃ nanofiber revealed photoluminescent peaks in the ultraviolet and visible ranges.

Fig. 6 FT-IR spectra of the as-prepared and calcined BaMnO₃ nanofibers



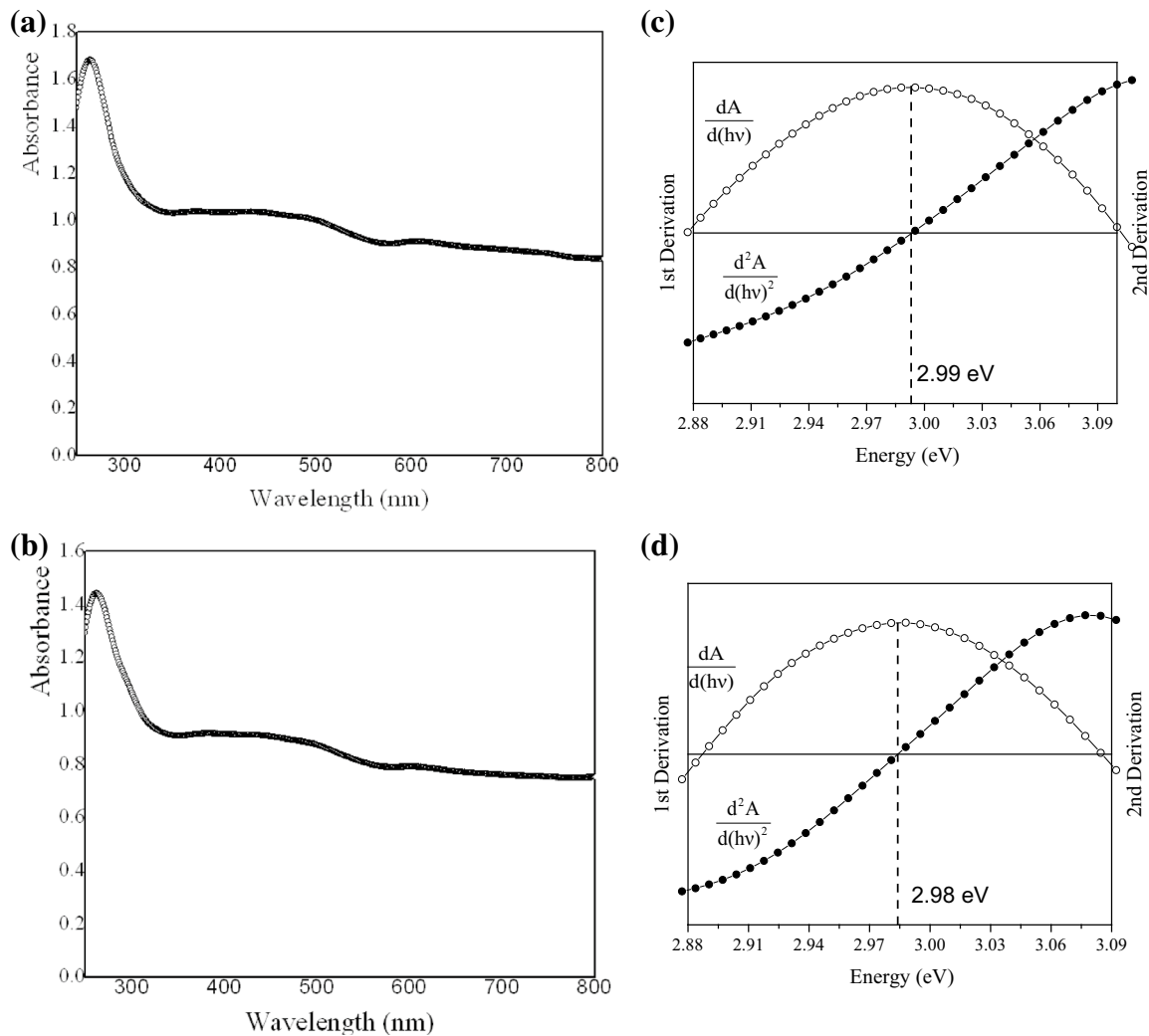


Fig. 7 The absorbance spectrum and the first and second derivatives of the absorbance data versus energy for BaMnO₃ nanofibers calcined at a 700 °C and **b** 800 °C. The first and the second derivatives of the absorbance data are shown in the images (c) and (d)

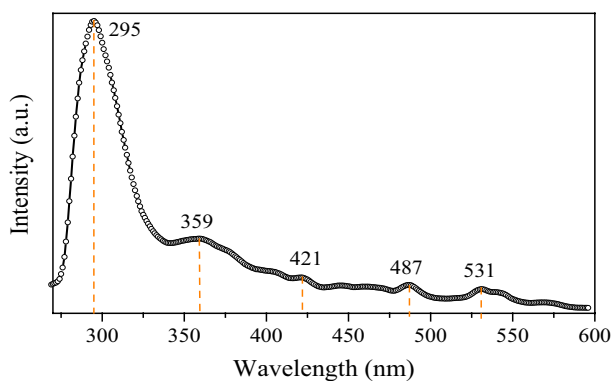


Fig. 8 Experimental PL spectrum of BaMnO₃ nanofibers

References

1. X.S. Peng, G.W. Meng, X.F. Wang, Y.W. Wang, J. Zhang, X. Liu, and L.D. Zhang, *Chem. Mater.* **14**, 4490 (2002)
2. D. Li, T. Herricks, Y. Xia, *Appl. Phys. Lett.* **83**, 4586 (2003)
3. S.J. Park, S. Bhargava, E.T. Bender, E.G.G. Chase, and R.D. Ramsier, *J. Mater. Res.* **23**, 1193 (2008)
4. K.R. Reddy, V.G. Gomes, and M. Hassan, *Mater. Res. Express* **1**, 015012 (2014)
5. T. Ramezanpour, H.M. Chenari, H. Ziyadi, *J. Mater. Sci. Mater. Electron.* **28**, 16226 (2017)
6. H.M. Chenari, and H. Kangarlou, *Phys. B* **499**, 38 (2016)
7. O. Rezaee, H.M. Chenari, F.E. Ghodsi, H. Ziyadi, *J. Alloys Compd.* **690**, 864 (2017)
8. R. Ramaseshan, S. Sundarajan, R. Jose, S. Ramakrishna, *J. Appl. Phys.* **102**, 7 (2007)
9. T.A. Kowalewski, S. Blonski, S. Barral, *Bull. Pol. Acad. Sci. Tech. Sci.* **53**, 385 (2005)
10. S. Ramakrishna, K. Fujihara, W.E. Teo, T. Yong, Z. Ma, and R. Ramaseshan, *Mater. Today* **9**, 40 (2006)

11. S.H. Xie, Y.Y. Liu, and J.Y. Li. *Front. Phys.* **7**, 399 (2012)
12. Y.W. Baji, Q. Mai, S.C. Li, Y. Wong, Liu, and Q.W. Yao, *Nanotechnology* **22**, 235702 (2011)
13. F.M. Gu, W.W. Pan, Q.F. Liu, J.B. Wang, *J. Phys. D Appl. Phys.* **46**, 445003 (2013)
14. G.N.S. Vijayakumar, M. Rathnakumari, and P. Sureshkumar, *Front. Mater. Sci.* **6**, 69 (2012)
15. K. Hayat, M.A. Rafiq, and M.M. Hasan, *Ceram. Int.* **38**, 1441 (2012)
16. K. Hayat, M.A. Rafiq, S.K. Durrani, and M.M. Hasan, *Phys. B* **406**, 309 (2011)
17. A. Querejeta, M. Varela, M. Parras, M. Monte, F.D. Garcia-Hernandez, and J.M.G. Calbet, *Chem. Mater.* **21**, 1898 (2009)
18. G.K. Williamson, and W.H. Hall, *Acta Metall.* **1**, 22 (1953)
19. A. Katoch, S.-W. Choi, S.S. Kim, *Metals Mater. Int.* **21**(2), 213–221 (2015)
20. J.Y. Park, S.-W. Choi, K. Asokan, S.S. Kim, *J. Nanosci. Nanotechnol.* **10**, 3604 (2010)
21. S. Balamurugan, K.S. Asha Mini, T.S. Raja, and P. Parthiban. *J. Nanosci. Nanotechnol.* **15**, 5978 (2015)
22. F. Gao, R.A. Lewis, X.L. Wang, and S.X. Dou. *J. Alloy. Compd.* **347**, 314 (2002)
23. C.G. Hu, H. Liu, C.S. Lao, L.Y. Zhang, D. Davidovic, and Z.L. Wang, *J. Phys. Chem. B* **110**, 14050 (2006)
24. H. Shibahara, H. Hashimoto, *J. Cryst. Growth* **65**, 683 (1983)
25. H. Shibahara, *J. Solid State Chem.* **81**, 40 (1989)
26. S. Deepa, S. Vidya, P.C. Manu, S. Solomon, A. John, J.K. Thomas, *J. Alloy. Compd.* **509**, 1830 (2011)